PHOTONICS Research

Effect of dispersion on indistinguishability between single-photon wave-packets

YUN-RU FAN,[1] CHEN-ZHI YUAN,[1,5] RUI-MING ZHANG,[1] SI SHEN,[1] PENG WU,[1] HE-QING WANG,[2] (iD)
HAO LI,[2] (iD) GUANG-WEI DENG,[1] HAI-ZHI SONG,[1,3] (iD) LI-XING YOU,[2] (iD) ZHEN WANG,[2] YOU WANG,[1,3,6]
GUANG-CAN GUO,[1,4] AND QIANG ZHOU[1,4,7] (iD)

[1]*Institute of Fundamental and Frontier Sciences, University of Electronic Science and Technology of China, Chengdu 610054, China*
[2]*Shanghai Institute of Microsystem and Information Technology, Chinese Academy of Sciences, Shanghai 200050, China*
[3]*Southwest Institute of Technical Physics, Chengdu 610041, China*
[4]*CAS Key Laboratory of Quantum Information, University of Science and Technology of China, Hefei 230026, China*
[5]*e-mail: c.z.yuan@uestc.edu.cn*
[6]*e-mail: youwang_2007@aliyun.com*
[7]*e-mail: zhouqiang@uestc.edu.cn*

With propagating through a dispersive medium, the temporal–spectral profile of optical pulses should be inevitably modified. Although such dispersion effect has been well studied in classical optics, its effect on a single-photon wave-packet has not yet been entirely revealed. In this paper, we investigate the effect of dispersion on indistinguishability between single-photon wave-packets through the Hong–Ou–Mandel (HOM) interference. By dispersively manipulating two weak coherent single-photon wave-packets which are prepared by attenuating mode-locked laser pulses before interfering with each other, we observe that the difference of the second-order dispersion between two optical paths of the HOM interferometer can be mapped to the interference curve, indicating that (i) with the same amount of dispersion effect in both paths, the HOM interference curve must be only determined by the intrinsic indistinguishability between the wave-packets, i.e., dispersion cancellation due to the indistinguishability between Feynman paths; and (ii) unbalanced dispersion effect in two paths cannot be canceled and will broaden the interference curve thus providing a way to measure the second-order dispersion coefficient. Our results suggest a more comprehensive understanding of the single-photon wave-packet and pave ways to explore further applications of the HOM interference. © 2021 Chinese Laser Press

https://doi.org/10.1364/PRJ.421180

1. INTRODUCTION

Similar to procedures for analyzing its classical counterpart, i.e., the electromagnetic wave, properties of single photons have been investigated through interference [1,2]. Exciting demonstrations, which certify the genuine quantum nature of single photons, have been realized [3–5]. One important genuine quantum nature is the indistinguishability between single-photon wave-packets, which has been characterized through Hong–Ou–Mandel (HOM) interference in different degrees of freedom of single-photon wave-packets, such as in spatial mode [6], temporal mode [7], polarization mode [8], spectral mode [9–11], and orbital angular momentum mode [12]. Moreover, the HOM interference is also applied to quantum communications with dispersive quantum channels, such as quantum teleportation [13,14] and measurement device independent key distribution [15–17]. Generally, the dispersion distortion should take place after a single-photon wave-packet propagating through dispersive environment.

For instance, the dispersion-induced temporal-mode broadening has been investigated with single-photon wave-packets in Ref. [18]. More importantly, the dispersion effect would also change the indistinguishability between single-photon wave-packets in the spectral–temporal profile, which has not yet been revealed so far.

In this work, we investigate the effect of dispersion on indistinguishability between single-photon wave-packets via the HOM interference and implement two proof-of-principle demonstrations with attenuated coherent single-photon wave-packets which are prepared by attenuating mode-locked laser pulses. Our analyses show that the difference of dispersion effect between the propagation paths of the two single-photon wave-packets can be mapped into the HOM interference curve. In one case, the mode-locked laser pulses propagate through a dispersion module, and then are separated into two parts which are attenuated to single-photon levels before sending them to a balanced HOM interferometer. Our results show that the

width of the HOM interference curve is independent with the dispersion from the dispersion module, i.e., dispersion cancellation [19–21] due to the indistinguishability between Feynman paths [22,23], thus restoring the original temporal width of the wave-packets. In another case, two attenuated coherent single-photon wave-packets are sent into an unbalanced HOM interferometer, i.e., different dispersion between optical interference paths. The unbalanced dispersion cannot be canceled and will modify the HOM interference curve. By measuring the change of the interference curve, we can obtain the second-order dispersion coefficient of the unbalanced dispersion, thus providing a new method for measuring it.

2. THEORETICAL MODEL AND ANALYSIS

Figure 1(a) gives the conceptual illustration of our proposed method. We consider two single-photon wave-packets with the pulse width of T_0, which propagate along path A and path B, respectively. Two dispersion modules are utilized to manipulate the spectral–temporal profiles of two wave-packets. Then the wave-packets are input into an HOM interferometer, consisting of a 50:50 beam splitter, two single photon detectors, and a coincidence circuit. To observe the HOM interference curve, an optical delay line is introduced in path B. The effect of dispersion on indistinguishability between two single-photon wave-packets is measured by comparing the HOM interference curves with different dispersive manipulations.

Assuming the two single-photon wave-packets propagating along paths A and B are both in coherent state, we can present their initial quantum state as [24]

$$|\psi_0\rangle_{A,B} = |\alpha_{A,B}(t)\rangle, \tag{1}$$

satisfying

$$a_{A,B}(t')|\alpha_{A,B}(t)\rangle_A = \alpha_{A,B}(t')|\alpha_{A,B}(t)\rangle \tag{2}$$

and

$$\alpha_{A,B}(t) = (T_0\sqrt{\pi})^{-1/2} e^{-\frac{t^2}{2T_0^2}}, \tag{3}$$

where $a_{A,B}(t)$ is the annihilation operators of fields in modes A or B, and the temporal amplitude function $\alpha_{A,B}(t)$ is assumed to be Gaussian. The coincidence count per trial $P(\tau)$ without any dispersion can be expressed by (see the derivations in Appendix A)

$$P(\tau) = 1 - \frac{1}{2} e^{-\frac{\tau^2}{2T_0^2}}, \tag{4}$$

where τ is the relative time delay between two optical paths. According to Eq. (4), Fig. 1(b) gives a conceptual HOM interference curve without dispersive manipulation and shows the cartoon process of how to obtain the HOM interference, in which the fixed single-photon wave-packet is indicated by solid lines (only shown with relative time delay being zero and omitted with other cases), while the moving one is indicated by
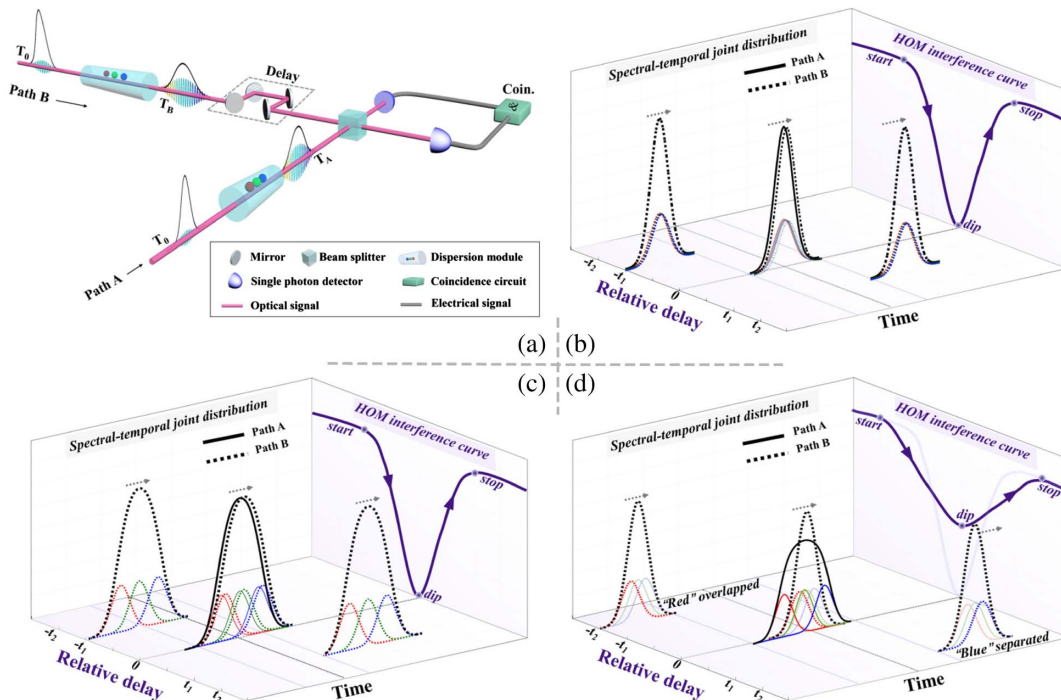

Fig. 1. Conceptual illustration of the HOM interference to reveal the dispersion effect on the indistinguishability between single-photon wave-packets. (a) HOM interferometer with dispersive manipulation modules. Two identical single-photon wave-packets are manipulated with dispersion modules along two optical paths, i.e., path A and path B, and then are sent into an HOM interferometer; (b) HOM interference curves without the second-order dispersion along two paths; (c) with the same second-order dispersion along two paths, i.e., balanced HOM interferometer; (d) with unbalanced second-order dispersions along two paths. To obtain the HOM interference curve, the travel time of the wave-packet in path A is fixed, and that in path B is varied and the time axis is in reference to the center of the pulse in path A. To guide eyes, envelopes of three sub-wave-packets are depicted with solid and dashed lines in red, green, and blue, respectively, and the black envelope covering the three sub-wave-packets is used to illustrate the widths of the wave-packets.

dashed lines. The HOM interference curve with a full width at half-maximum (FWHM) which is $\sqrt{2}$ times of the FWHM of the two single-photon wave-packets can be obtained by scanning τ from $-t_1$ to t_1 in the axis of relative delay.

After the dispersive manipulation of a single-photon wave-packet, one may expect the interference curve to be changed due to the group-velocity time delay and the second-order dispersion effect, respectively. Ignoring the third- and higher-order dispersion effects, we can obtain the coincidence count per trial $P'(\tau)$, as given by (see the derivations in Appendix A)

$$P'(\tau) = 1 - \frac{T_0^2}{\sqrt{4T_0^4 + \alpha^2}} e^{-\frac{2(\tau - \delta\tau)^2}{4T_0^2 + (\alpha/T_0)^2}}, \tag{5}$$

where $\delta\tau = \beta_A^{(1)}(0)L_A - \beta_B^{(1)}(0)L_B$ and $\alpha = \beta_A^{(2)}(0)L_A - \beta_B^{(2)}(0)L_B$ represent the difference of group-velocity time delay and the difference of the group-velocity dispersion introduced by two optical paths respectively, with $\beta_A^{(1)}(0)$ or $\beta_B^{(1)}(0)$, $\beta_A^{(2)}(0)$ or $\beta_B^{(2)}(0)$, and L_A or L_B being the inverse group-velocity, group-velocity dispersion parameter, and the length of the dispersive path A or B.

Equation (5) gives the possible phenomena that would take place with dispersive manipulation. Such phenomena are further depicted in Figs. 1(c) and 1(d). In our cartoonish picture, the single-photon wave-packets are composed of three frequency components which are shown in red, green, and blue lines, respectively. Figure 1(c) indicates the situation that the two single-photon wave-packets experience the same amount of dispersion. Although for each wave-packet, different components in frequency are separated in the time domain after the dispersive manipulation—temporal broadening, the HOM interference only occurs with components in the same color, i.e., with the relative time delay from $-t_1$ to t_1— the same as the case shown in Fig. 1(b), which corresponds to the original width of the wave-packets. On the other hand, the situation for two wave-packets experiencing different amounts of dispersion is given in Fig. 1(d). In this case, both of them are also broadened in the time domain with different amounts, resulting in being partially distinguishable. The HOM interference can still happen due to the residual indistinguishability between them when the components in the same frequency are overlapping, leading to a wider HOM interference curve

with a smaller visibility. The corresponding changes of the HOM interference curve are determined by the different amount of dispersion experienced by the two wave-packets, given by Eq. (6):

$$\alpha = T_0 \sqrt{d^2/2 \ln 2 - 4T_0^2}, \tag{6}$$

where d is the FWHM of the HOM interference curve (see the derivations in Appendix A). Therefore, the different amount of dispersion can be obtained by measuring the width of the HOM interference curve.

3. PROOF-OF-PRINCIPLE DEMONSTRATIONS

Our proof-of-principle experimental setup is shown in Fig. 2 (see more details in Appendix B). In the demonstrations, single-photon wave-packets are attenuated from mode-locked laser pulses (PFL-200 M, Alnair Labs), with a mean photon number of 0.007 per pulse. The pulse width is 1.12 ± 0.01 ps, measured by a second-order autocorrelator (FEMTOCHROME, FR-103XL), and the repetition period T is 25 ns. The dispersive manipulation is realized by using pieces of fiber as dispersion modules.

We first measure the HOM interference curve at the output port of a mode-locked laser as shown in Fig. 2, which is used as a reference for our demonstrations. The HOM interference curve is obtained as shown in Fig. 3(a). The blue dots are the normalized measured data, and the solid lines are the Gaussian fitting curves obtained by the Monte Carlo method [25], in which 1000-time random sampling is performed around the measured data assumed to be Poissonian. By averaging the FWHM of the 1000 fitting curves, we obtain that the FWHM of the HOM-dip is 1.31 ± 0.01 ps with the visibility of $50.2\% \pm 0.2\%$, suggesting a width of 0.93 ± 0.01 ps for laser pulses.

Next, we connect a dispersion module (50 km long single-mode fiber spool, Yangtze Optical Fibre and Cable Co., Ltd., G.652.D ULL) at the output port of our mode-locked laser. After propagating through this dispersive environment, the laser pulses would be broadened to about 3.0 ns with a second-order dispersion coefficient of 17.0 ps/(km · nm). We employ a superconducting nanowire single photon detector (SNSPD, Photon Technology Co., P-CS-6) [26] and a time
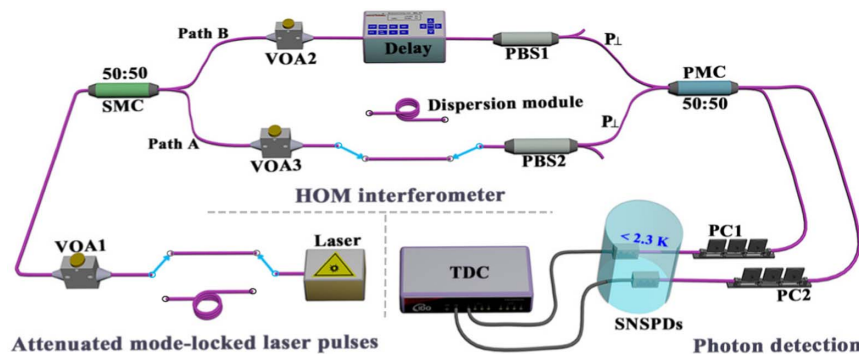

Fig. 2. Experimental setup. The setup consists of attenuated mode-locked laser pulses, HOM interferometer, and photon detection with a dispersion module. VOA, variable optical attenuator; SMC, single-mode fiber coupler; PBS, polarization beam splitter; PMC, polarization-maintaining fiber coupler; PC, polarization controller; SNSPD, superconducting nanowire single photon detector; TDC, time to digital convertor.
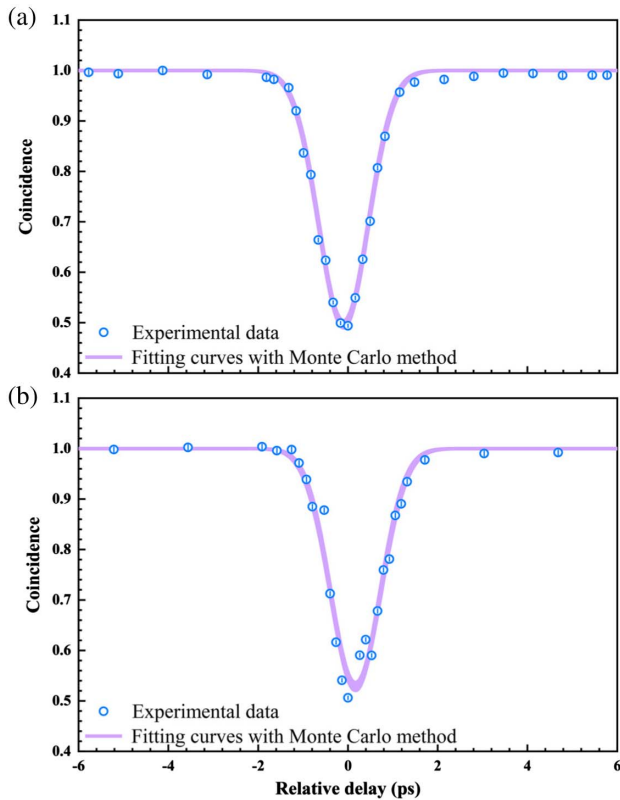
(a)

(b)

Fig. 3. HOM interference curves (a) without a dispersion module, and (b) with 50 km long fiber as the dispersion module at the output of the mode-locked laser, respectively. The blue dots are experimental results. The solid purple lines are Gaussian fitting curves obtained via Monte Carlo method with 1000-time random sampling around each measured data assumed as Poissonian distribution.

to digital converter (TDC, ID Quantique, ID900) to measure the width of the broadened laser pulses after being attenuated to single-photon level. After the dispersive manipulation, the measured pulse width is 3.4 ± 0.3 ns including a time jitter of the SNSPD and TDC (see more details in Fig. 5 in Appendix B). However, the width of the measured HOM interference curve is 1.31 ± 0.01 ps with the visibility of $47.2\% \pm 0.2\%$, as shown in Fig. 3(b), which is nearly the same as that without the dispersive manipulation. The degraded visibility could be attributed to the unbalanced mean photon number in two paths of HOM interferometer. This phenomenon would be explained as dispersion cancellation, i.e., the result of HOM interference is immune to the dispersion effect on the individual wave-packet. The dispersion cancellation—including the dispersion related chirp effect [27,28]—has also been demonstrated with correlated photon pairs, in which the dispersion cancellation is attributed to the nonlocal property of entanglement. In our case, the dispersion cancellation phenomenon is related to the HOM interference-based entangled N00N state generation [29–33], and can also be explained with the Feynman diagram, i.e., we cannot tell which Feynman path the single-photon wave-packet is from even with dispersive manipulation. Therefore, the HOM interference must recover the original width of the dispersively

manipulated wave-packet, offering us a dispersion immune method to measure the original width of laser pulses. Although the HOM interference scheme has been used to measure the width of ultrashort laser pulses since 1993 [34], the dispersion influence on such a measurement has not yet been discussed, which is addressed in this work.

The pulse width from the HOM interference is 0.93 ± 0.01 ps, which is smaller than 1.12 ± 0.01 ps obtained from the second-order autocorrelation measurement [35]. This would be caused by the dispersive broadening before the second-order autocorrelation measurement. It is worth noting that the total time jitter from the SNSPDs and TDC is remarkably shorter than the width of pulses after dispersion. Thus, our coincidence detection system is capable of working in a time-resolved manner and revealing the detailed structure in coincidence counts versus photon detection time delay [36,37]. In our experiment, we set the width of the coincidence window wider than the dispersed pulse width to obtain the coincidence counts for the HOM interference curve as shown in Fig. 3(b), i.e., our HOM interference curve is measured in a time-unresolved manner.

Then, we use another dispersion module (80 m long single-mode fiber, SMF-28) to serve as the unknown optical material, which is inserted in one arm of the HOM interferometer as shown in Fig. 2. One may think that an extra optical path should be added in the other arm to balance transmission times in two arms. Fortunately, the extra optical path can be removed according to the result reported in Ref. [38], i.e., the HOM interference can occur between periodically delayed mode-locked laser pulses. In our experiment, the HOM interference curves are measured between laser pulses with a 16-period delay. The measured results are shown in Fig. 4. The FWHM of HOM interference curves is 3.76 ± 0.08 ps with the visibility of $16.6\% \pm 0.3\%$, which is consistent with our theoretical predictions, 3.96 ps and 16.5%, respectively. According to Eq. (4), the second-order dispersion coefficient of our measured 80 m long fiber is 16.3 ± 0.5 ps/(km · nm), which is in consistence with the dispersion parameter from the manufacturer within errors, i.e., 17.0 ps/(km · nm).
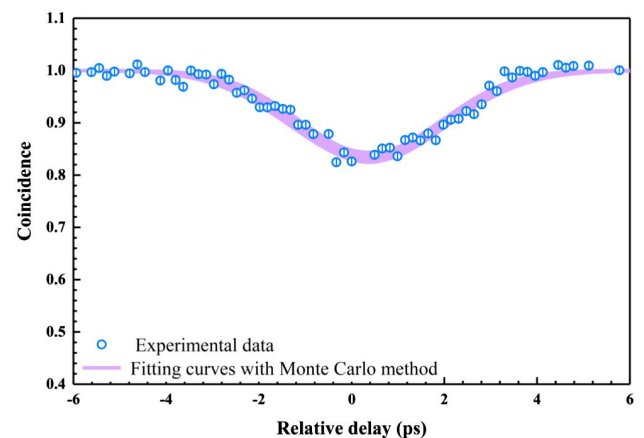

Fig. 4. HOM interference curves with a 80 m long single-mode fiber inserted in one path, which corresponds to 16 periods of mode-locked laser pulses.

4. DISCUSSION AND CONCLUSIONS

Several methods have been demonstrated to measure the second-order dispersion coefficient of optical media, for instance, the time of flight [39], phase shift [40], and interferometric methods [41]. In the former two methods, the response time or time jitter of electronics limits the measurement precision [42]. As for the interferometric methods, the second-order dispersion coefficient is obtained from the first-order interference, which is phase sensitive. In our method, the second-order dispersion is measured by the HOM interference, which is insensitive in phase [43]. One may concern that the statistical properties of the HOM method would influence the precision of our measurement. To address this, in our demonstration the measured results are not straightly extracted from the photon counting results, but the Monte Carlo method fitted curves. The results are shown in Figs. 3 and 4; the solid purple lines indicate 1000-time Monte Carlo fitting curves. It can be seen that such a method achieves a precision of 10 fs for the pulse width and a precision as high as 0.5 ps/(km · nm) for the second-order dispersion coefficient measurement.

In summary, we have investigated the effect of dispersion on indistinguishability between single-photon wave-packets via HOM interference. From the perspective of Feynman paths, the indistinguishability is independent of the same dispersive manipulation and only related to the unbalanced dispersion effect in two optical paths of the HOM interferometer. Our proof-of-principle demonstrations have proved that such a scheme can be used to measure the original pulse width of ultrashort laser pulses even after propagating through the dispersive environment, i.e., dispersion immunity, and to measure the second-order dispersion coefficient of an unknown optical material. The results show that the measurement precision can reach 10 fs and 0.5 ps/(km · nm) for the measurement of the pulse width and the second-order dispersion, respectively. Furthermore, our study provides a deeper understanding for single-photon wave-packets and opens up new applications for HOM interference.

Note added: A similar dispersion effect on single-photon wave-packets has recently been reported for single photons generated from the spontaneous parametric downconversion process [44].

APPENDIX A: THEORETICAL MODEL

The paths A and B in Fig. 1(a) are defined as spatial modes A and B, respectively. Assuming the single-photon wave-packets in spatial modes A and B are both in coherent state, we can present their initial quantum state as [24]

$$|\psi_0\rangle_{A,B} = |\alpha_{A,B}(t)\rangle, \tag{A1}$$

satisfying

$$a_{A,B}(t')|\alpha_{A,B}(t)\rangle = \alpha_{A,B}(t')|\alpha_{A,B}(t)\rangle, \tag{A2}$$

and

$$\int dt |\alpha_{A,B}(t)|^2 = |\alpha_{A0,B0}|^2, \tag{A3}$$

where $a_{A,B}(t')$ is the annihilation operator of field in modes A or B, and $|\alpha_{A0,B0}|^2$ is the averaged photon number in each wave-packet. After passing through the dispersive media in the propagation pathways, the coherent state evolves from Eq. (A1) into

$$|\psi_1\rangle_{A,B} = |\alpha_{A1,B1}(t)\rangle, \tag{A4}$$

where

$$\alpha_{A1,B1}(t)$$
$$= (2\pi)^{-1/2} \int d\Omega_{A,B} \alpha_{A,B}(\Omega_{A,B}) e^{-i(\omega_0+\Omega_{A,B})t + i\beta_{A,B}(\Omega_{A,B})L_{A,B}}, \tag{A5}$$

with $\alpha_{A,B}(\Omega_{A,B}) = (2\pi)^{-1/2} \int dt \alpha_{A,B}(t) e^{i(\omega_0+\Omega_{A,B})t}$ and the central angular frequency of the two wave-packets both assumed to be ω_0. In Eq. (A5), $L_{A,B}$ and $\beta_{A,B}$ are the length of the dispersive medium on path A or B, and the corresponding propagation constant at angular frequency of $\omega_0 + \Omega_{A,B}$. Before being incident on the beam splitter in Fig. 1(a), the wave-packet in mode B is delayed by τ and its quantum state turns into

$$|\psi_2\rangle_B = |\alpha_{B1}(t+\tau)\rangle_B. \tag{A6}$$

Introducing spatial modes C and D corresponding to the two output ports of the beam splitter, we can obtain the annihilation operators $a_{C,D}(t)$ of fields in the two modes via the transforms

$$a_C(t) = 2^{-1/2}[a_A(t) + a_B(t)], \tag{A7}$$

$$a_D(t) = 2^{-1/2}[a_A(t) - a_B(t)]. \tag{A8}$$

The second-order correlation between fields in modes C and D can be obtained as

$$G_{C,D}^{(2)}(t, t+\tau_c)$$
$$= {}_A\langle\psi_1|_B\langle\psi_2|a_C^\dagger(t)a_D^\dagger(t+\tau_c)a_D(t+\tau_c)a_C(t)|\psi_2\rangle_B|\psi_1\rangle_A, \tag{A9}$$

where τ_c is the time delay introduced in calculating the second-order correlation function. Then, we can calculate the coincidence counts between the photons detected in modes C and D as

$$n_{CD}(\tau) = \eta_C\eta_D \int_{T_1}^{T_2} dt \int_{-\Delta\tau_{c0}/2}^{\Delta\tau_{c0}/2} d\tau_c G_{C,D}^{(2)}(t, t+\tau_c), \tag{A10}$$

where $\eta_{C,D}$ summarize the collection and detection efficiencies of the photons; T_1 and T_2 are the start and stop times of the coincidence counting measurement; and $\Delta\tau_{c0}$ is the width of the coincidence counting window. After substituting Eqs. (A7)–(A9) into Eq. (A10), $n_{CD}(\tau)$ comprises eight terms possible to be nonzero. We can list them as

(i)

$$n_{CD,1}(\tau) = \frac{\eta_C\eta_D}{4} \int_{T_1}^{T_2} dt \int_{-\Delta\tau_{c0}/2}^{\Delta\tau_{c0}/2} d\tau_c {}_A\langle\psi_1|_B\langle\psi_2|a_A^\dagger(t)a_A^\dagger(t+\tau_c)a_A(t+\tau_c)a_A(t)|\psi_2\rangle_B|\psi_1\rangle_A$$
$$= \frac{\eta_C\eta_D}{4} \int_{T_1}^{T_2} dt \int_{-\Delta\tau_{c0}/2}^{\Delta\tau_{c0}/2} d\tau_c |\alpha_{A1}(t)|^2|\alpha_{A1}(t+\tau_c)|^2 \approx \frac{\eta_C\eta_D}{4}|\alpha_{A0}|^4. \tag{A11}$$

(ii)

$$n_{CD,2}(\tau) = \frac{\eta_C \eta_D}{4} \int_{T_1}^{T_2} dt \int_{-\Delta\tau_{c0}/2}^{\Delta\tau_{c0}/2} d\tau_{cA} \langle \psi_1|_B \langle \psi_2| a_B^\dagger(t) a_B^\dagger(t+\tau_c) a_B(t+\tau_c) a_B(t) |\psi_2\rangle_B |\psi_1\rangle_A$$

$$= \frac{\eta_C \eta_D}{4} \int_{T_1}^{T_2} dt \int_{-\Delta\tau_{c0}/2}^{\Delta\tau_{c0}/2} d\tau_c |\alpha_{B1}(t)|^2 |\alpha_{B1}(t+\tau_c)|^2 \approx \frac{\eta_C \eta_D}{4} |\alpha_{B0}|^4. \tag{A12}$$

At the last step in Eq. (A12), we assume that $T_2 - T_1$ and $\Delta\tau_{c0}$ are both remarkably larger than the temporal width of the dispersion-broadened wave-packets, and this is easily satisfied in our experiment. It is obvious that $n_{CD,1}(\tau)$ and $n_{CD,2}(\tau)$ originate from the second-order autocorrelation of the two wave-packets, respectively. In fact, in a Hanbury–Brown–Twiss experiment, the normalized second-order autocorrelation function of the two wave-packets is

$$g_{A,B}^{(2)}(\tau_c) = \frac{\int_{T_1}^{T_2} dt \int_{\tau_c - \Delta\tau_{c0}/2}^{\tau_c + \Delta\tau_{c0}/2} d\tau'_{cA,B} \langle \psi_{1,2}| a_A^\dagger(t) a_A^\dagger(t+\tau'_c) a_A(t+\tau'_c) a_A(t) |\psi_{1,2}\rangle_{A,B}}{\left[\int_{T_1}^{T_2} dt_{A,B} \langle \psi_{1,2}| a_A^\dagger(t) a_A(t) |\psi_{1,2}\rangle_{A,B} \right]^2}. \tag{A13}$$

Thus, general forms of $n_{CD,1}(\tau)$ and $n_{CD,2}(\tau)$ are

$$n_{CD,1}(\tau) = \frac{\eta_C \eta_D}{4} g_A^{(2)}(0) \left[\int_{T_1}^{T_2} dt_A \langle \psi_1| a_A^\dagger(t) a_A(t) |\psi_1\rangle_A \right]^2, \tag{A14}$$

and

$$n_{CD,2}(\tau) = \frac{\eta_C \eta_D}{4} g_B^{(2)}(0) \left[\int_{T_1}^{T_2} dt_B \langle \psi_2| a_B^\dagger(t) a_B(t) |\psi_2\rangle_B \right]^2. \tag{A15}$$

Since we assume the single-photon wave-packets are in coherent state, $g_{A,B}^{(2)}(0) = 1$ and therefore the results in Eq. (A11) [Eq. (A12)] and Eq. (A14) [Eq. (A15)] are consistent with each other.

(iii)

$$n_{CD,3}(\tau) = -\frac{\eta_C \eta_D}{4} \int_{T_1}^{T_2} dt \int_{-\Delta\tau_{c0}/2}^{\Delta\tau_{c0}/2} d\tau_{cA} \langle \psi_1|_B \langle \psi_2| a_A^\dagger(t) a_A^\dagger(t+\tau_c) a_B(t+\tau_c) a_B(t) |\psi_2\rangle_B |\psi_2\rangle_A$$

$$= -\frac{\eta_C \eta_D}{4} \int_{T_1}^{T_2} dt \int_{-\Delta\tau_{c0}/2}^{\Delta\tau_{c0}/2} d\tau_c \alpha_{A1}^*(t) \alpha_{A1}^*(t+\tau_c) \alpha_{B2}(t+\tau_c) \alpha_{B2}(t)$$

$$= -\frac{\eta_C \eta_D}{4} (2\pi)^{-2} e^{-i2\omega_0 \tau} \int_{T_1}^{T_2} dt \int_{-\Delta\tau_{c0}/2}^{\Delta\tau_{c0}/2} d\tau_c \int d\Omega_A \int d\Omega'_A \int d\Omega_B \int d\Omega'_B$$

$$\times \alpha_A^*(\Omega_A) \alpha_A^*(\Omega'_A) \alpha_B(\Omega_B) \alpha_B(\Omega'_B)$$

$$\times e^{i(\Omega_A + \Omega'_A - \Omega_B - \Omega'_B)t + i(\Omega'_A - \Omega_B)\tau_c - i[\beta_A(\Omega_A)L_A + \beta_A(\Omega'_A)L_A - \beta_B(\Omega_B)L_B - \beta_A(\Omega'_B)L_A]}$$

$$= -\frac{\eta_C \eta_D}{4} e^{-i2\omega_0 \tau} \left\{ \int d\Omega_A \alpha_A^*(\Omega_A) \alpha_B(\Omega_A) e^{-i[\beta_A(\Omega_A)L_A - \beta_B(\Omega_A)L_B]} \right\}^2. \tag{A16}$$

(iv)

$$n_{CD,4}(\tau) = -\frac{\eta_C \eta_D}{4} \int_{T_1}^{T_2} dt \int_{-\Delta\tau_{c0}/2}^{\Delta\tau_{c0}/2} d\tau_{cA} \langle \psi_1|_B \langle \psi_2| a_B^\dagger(t) a_B^\dagger(t+\tau_c) a_A(t+\tau_c) a_A(t) |\psi_2\rangle_B |\psi_1\rangle_A$$

$$= -\frac{\eta_C \eta_D}{4} \int_{T_1}^{T_2} dt \int_{-\Delta\tau_{c0}/2}^{\Delta\tau_{c0}/2} d\tau_c \alpha_{B2}^*(t) \alpha_{B2}^*(t+\tau_c) \alpha_{A1}(t+\tau_c) \alpha_{A1}(t)$$

$$= -\frac{\eta_C \eta_D}{4} (2\pi)^{-2} e^{-i2\omega_0 \tau} \int_{T_1}^{T_2} dt \int_{-\Delta\tau_{c0}/2}^{\Delta\tau_{c0}/2} d\tau_c \int d\Omega_A \int d\Omega'_A \int d\Omega_B \int d\Omega'_B$$

$$\times \alpha_B^*(\Omega_B) \alpha_B^*(\Omega'_B) \alpha_A(\Omega_A) \alpha_A(\Omega'_A) e^{i(\Omega_B + \Omega'_B - \Omega_A - \Omega'_A)t + i(\Omega'_B - \Omega_A)\tau_c [\beta_B(\Omega_B)L_B + \beta_B(\Omega'_B)L_B - \beta_A(\Omega_A)L_A - \beta_A(\Omega'_A)L_A]}$$

$$= -\frac{\eta_C \eta_D}{4} e^{i2\omega_0 \tau} \left\{ \int d\Omega_A \alpha_B^*(\Omega_A) \alpha_A(\Omega_A) e^{-i[\beta_B(\Omega_A)L_B - \beta_A(\Omega_A)L_A]} \right\}^2. \tag{A17}$$

It is obvious that the terms $n_{CD,3}(\tau)$ and $n_{CD,4}(\tau)$ oscillate quickly with variable τ, and their sum is

$$n_{CD,3}(\tau) + n_{CD,4}(\tau) = -\frac{\eta_C \eta_D}{2} \cos(2\omega_0 \tau) \text{Re} \left\{ \int d\Omega_A \alpha_B^*(\Omega_A) \alpha_A(\Omega_A) e^{-i[\beta_B(\Omega_A)L_B - \beta_A(\Omega_A)L_A]} \right\}^2. \tag{A18}$$

The oscillating period of the term $\cos(2\omega_0\tau)$ is smaller than 1 fs for the light field used in our experiment. In our experimental system, especially the one with optical fiber devices, the fluctuation of optical depth makes τ vary quickly with respect to the time scale of $T_2 - T_1$ and therefore $n_{CD,3}(\tau) + n_{CD,4}(\tau)$ in Eq. (A18) turns to be zero.

(v)

$$n_{CD,5}(\tau) = \frac{\eta_C\eta_D}{4}\int_{T_1}^{T_2}dt\int_{-\Delta\tau_{c0}/2}^{\Delta\tau_{c0}/2}d\tau_{cA}\langle\psi_1|_B\langle\psi_2|a_A^\dagger(t)a_B^\dagger(t+\tau_c)a_B(t+\tau_c)a_A(t)|\psi_2\rangle_B|\psi_1\rangle_A$$
$$= \frac{\eta_C\eta_D}{4}\int_{T_1}^{T_2}dt\int_{-\Delta\tau_{c0}/2}^{\Delta\tau_{c0}/2}d\tau_c|\alpha_{A1}(t)|^2|\alpha_{B2}(t+\tau_c)|^2 \approx |\alpha_{A0}|^2|\alpha_{B0}|^2.$$

(A19)

(vi)

$$n_{CD,6}(\tau) = \frac{\eta_C\eta_D}{4}\int_{T_1}^{T_2}dt\int_{-\Delta\tau_{c0}/2}^{\Delta\tau_{c0}/2}d\tau_{cA}\langle\psi_1|_B\langle\psi_2|a_B^\dagger(t)a_A^\dagger(t+\tau_c)a_A(t+\tau_c)a_B(t)|\psi_2\rangle_B|\psi_1\rangle_A$$
$$= \frac{\eta_C\eta_D}{4}\int_{T_1}^{T_2}dt\int_{-\Delta\tau_{c0}/2}^{\Delta\tau_{c0}/2}d\tau_c|\alpha_{A1}(t+\tau_c)|^2|\alpha_{B2}(t)|^2 \approx |\alpha_{A0}|^2|\alpha_{B0}|^2.$$

(A20)

At the last step in Eq. (A12), the assumption that $T_2 - T_1$ and $\Delta\tau_{c0}$ are remarkably larger than the temporal width of the dispersion-broadened wave-packets is used again.

(vii)

$$n_{CD,7}(\tau) = -\frac{\eta_C\eta_D}{4}\int_{T_1}^{T_2}dt\int_{-\Delta\tau_{c0}/2}^{\Delta\tau_{c0}/2}d\tau_{cA}\langle\psi_1|_B\langle\psi_2|a_A^\dagger(t)a_B^\dagger(t+\tau_c)a_A(t+\tau_c)a_B(t)|\psi_2\rangle_B|\psi_1\rangle_A$$
$$= -\frac{\eta_C\eta_D}{4}(2\pi)^{-2}\int_{T_1}^{T_2}dt\int_{-\Delta\tau_{c0}/2}^{\Delta\tau_{c0}/2}d\tau_c\alpha_{A1}^*(t)\alpha_{B2}^*(t+\tau_c)\alpha_{A1}(t+\tau_c)\alpha_{B2}(t)$$
$$= -\frac{\eta_C\eta_D}{4}(2\pi)^{-2}\int_{T_1}^{T_2}dt\int_{-\Delta\tau_{c0}/2}^{\Delta\tau_{c0}/2}d\tau_c\int d\Omega_A\int d\Omega_A'\int d\Omega_B\int d\Omega_B'\alpha_A^*(\Omega_A)\alpha_B^*(\Omega_B)\alpha_A(\Omega_A')\alpha_B(\Omega_B')$$
$$\times e^{i(\Omega_A-\Omega_B'+\Omega_B-\Omega_A')t+i(\Omega_B-\Omega_A')\tau_c+i(\Omega_B-\Omega_B')\tau-i[\beta_B(\Omega_B')L_B-\beta_B(\Omega_B)L_B+\beta_A(\Omega_A')L_A-\beta_A(\Omega_A)L_A]}$$
$$= -\frac{\eta_C\eta_D}{4}\left|\int d\Omega\alpha_A^*(\Omega)\alpha_B(\Omega)e^{-i\Omega\tau+i[\beta_A(\Omega)L_A-\beta_B(\Omega)L_B]}\right|^2.$$

(A21)

(viii)

$$n_{CD,8}(\tau) = -\frac{\eta_C\eta_D}{4}\int_{T_1}^{T_2}dt\int_{-\Delta\tau_{c0}/2}^{\Delta\tau_{c0}/2}d\tau_{cA}\langle\psi_1|_B\langle\psi_2|a_B^\dagger(t)a_A^\dagger(t+\tau_c)a_B(t+\tau_c)a_A(t)|\psi_2\rangle_B|\psi_1\rangle_A$$
$$= -\frac{\eta_C\eta_D}{4}(2\pi)^{-2}\int_{T_1}^{T_2}dt\int_{-\Delta\tau_{c0}/2}^{\Delta\tau_{c0}/2}d\tau_c\alpha_{B2}^*(t)\alpha_{A1}^*(t+\tau_c)\alpha_{B2}(t+\tau_c)\alpha_{A1}(t)$$
$$= -\frac{\eta_C\eta_D}{4}\left|\int d\Omega\alpha_A^*(\Omega)\alpha_B(\Omega)e^{-i\Omega\tau+i[\beta_A(\Omega)L_A-\beta_B(\Omega)L_B]}\right|^2.$$

(A22)

After summing Eqs. (A11), (A12), and (A16)–(A22) up, we can finally get

$$n(\tau) = \frac{\eta_C\eta_D|\alpha_{A0}|^2|\alpha_{B0}|^2}{4}\left\{\frac{|\alpha_{A0}|^2}{|\alpha_{B0}|^2}+\frac{|\alpha_{B0}|^2}{|\alpha_{A0}|^2}+2-\frac{2}{|\alpha_{A0}|^2|\alpha_{B0}|^2}\right.$$
$$\left.\times\left|\int d\Omega\alpha_A^*(\Omega)\alpha_B(\Omega)e^{-i[\Omega\tau+\beta_A(\Omega)L_A-\beta_B(\Omega)L_B]}\right|^2\right\}.$$

(A23)

Now, we introduce some assumptions for conveniently comparing Eq. (A23) to the experiments. First, the averaged photon numbers in the two single-photon wave-packets are both 1, i.e., $|\alpha_{A0}|^2 = |\alpha_{B0}|^2 = 1$. For convenience, α_{A0} and α_{B0} are treated as 1. Second, the single-photon wave-packets before passing through the dispersive medium are indistinguishable, and their temporal profile is Gaussian, i.e.,

$$\alpha_{A,B}(t) = (T_0\sqrt{\pi})^{-1/2}e^{-\frac{t^2}{2T_0^2}}.$$

(A24)

Third, the effect of higher-order dispersions is negligible, and $\beta_{A,B}(\Omega)$ can be approximated by truncating the Taylor expansion to the second order, i.e.,

$$\beta_{A,B}(\Omega) \approx \beta_{A,B}(0) + \beta_{A,B}^{(1)}(0)\Omega + \beta_{A,B}^{(2)}(0)\Omega^2,$$

(A25)

where $\beta_{A,B}^{(1)}(0)$ and $\beta_{A,B}^{(2)}(0)$ are the inverse group-velocity and group-velocity dispersion parameter of the dispersive path A (B), respectively.

Under the three assumptions above, Eq. (A23) gets

$$n(\tau) = \eta_C \eta_D \left\{ 1 - \frac{T_0^2}{\sqrt{4T_0^4 + \alpha^2}} e^{-2(\tau-\delta\tau)^2/[4T_0^2+(\alpha/T_0)^2]} \right\},$$

(A26)

where $\delta\tau = \beta_A^{(1)}(0)L_A - \beta_B^{(1)}(0)L_B$ and $\alpha = \beta_A^{(2)}(0)L_A - \beta_B^{(2)}(0)L_B$. It is obvious that the coincidence count per trial $P(\tau)$ can be obtained by normalizing $n(\tau)$ in Eq. (A26), i.e.,

$$P(\tau) = 1 - \frac{T_0^2}{\sqrt{4T_0^4 + \alpha^2}} e^{-2(\tau-\delta\tau)^2/[4T_0^2+(\alpha/T_0)^2]}.$$ **(A27)**

In Eq. (A27), the $P(\tau)$ versus τ forms the HOM interference curve and shows a dip centering at $\tau = \delta\tau$. The FWHM of this dip is

$$d = 2\sqrt{\ln 4}\sqrt{T_0^2 + (\alpha/2T_0)^2}.$$ **(A28)**

The visibility of the HOM-dip is given by

$$V = \frac{P_{\max}(\tau) - P_{\min}(\tau)}{P_{\max}(\tau)} = \frac{T_0^2}{\sqrt{4T_0^4 + \alpha^2}},$$ **(A29)**

where $P(\tau)_{\max}$ or $P(\tau)_{\min}$ is the maximum or minimum of versus τ.

When the two wave-packets experience identical dispersion, i.e., $\delta\tau = 0$ and $\alpha = 0$, Eq. (A16) degrades to

$$P(\tau) = 1 - \frac{1}{2} e^{-\tau^2/(2T_0^2)}.$$ **(A30)**

Thus, the FWHM of the HOM-dip is

$$d = 2\sqrt{\ln 4}\, T_0 = \sqrt{2} T_{\mathrm{FWHM}},$$ **(A31)**

where T_{FWHM} is the FWHM of the wave-packets, and the visibility equals 0.5. If we let $\beta_{A,B}(\Omega) = 0$, i.e., there does not exist dispersion along the propagation pathways of the two wave-packets, we can get an expression of $P(\tau)$ identical to Eq. (A30). This indicates that the HOM interference curve will not be affected by the balanced dispersion experienced by the two wave-packets. Therefore, we can obtain the original width of the single-photon wave-packet as $1/\sqrt{2}$ times the HOM

interference curve even though the wave-packets have been broadened significantly by the dispersive manipulation. According to Eq. (A28), when the dispersive manipulation in two paths is unbalanced, the difference of the second-order dispersion effect between two paths can accurately be mapped to the HOM interference curve by

$$\alpha = T_0 \sqrt{d^2/2 \ln 2 - 4T_0^2},$$ **(A32)**

which can be utilized to measure the second-order dispersion effect of an unknown optical material.

APPENDIX B: DETAILS OF THE EXPERIMENTAL SETUP

In the experiment setup shown in Fig. 2, the pulsed light source is selected as a passively mode-locked fiber laser (PFL-200M, Alnair Labs) with the central wavelength of 1548.74 nm, pulse duration of 1.12 ± 0.01 ps measured by the second-order autocorrelation method, repetition rate of 40 MHz, and 3 dB spectral bandwidth of 3.48 nm, as shown in Fig. 5(a). The laser pulses are attenuated to single-photon level with the mean photon number of 0.007 per wave-packet through a variable optical attenuator (VOA1, VOA2, and VOA3). To create two single-photon wave-packets, a 50:50 single-mode fiber coupler is used to divide the attenuated laser pulses into two parts propagating along two paths. Two wave-packets are injected into an HOM interferometer, which consists of the two variable optical attenuators (VOA2 and VOA3), two polarization beam splitters (PBS1 and PBS2), a 50:50 polarization-maintaining fiber coupler, and a fiber pigtailed variable optical delay line (Delay), as shown in Fig. 2. We can adjust the VOA2 and VOA3 in the two arms of the HOM interferometer to ensure that the mean photon numbers in the two paths are the same. The two PBS1 and PBS2 are used to ensure the polarization indistinguishability between the two wave-packets. A relative time delay between the two arms in the HOM interferometer is introduced by an optical delay line (MDL-002, General Photonics) with the accuracy of 10 fs and maximum time delay of 560 ps. Two output ports of the HOM interferometer are connected with two SNSPDs with detection efficiency of 68%. The electronic signals generated in photon detection events are input into a TDC (ID 900, ID Quantique) to obtain the
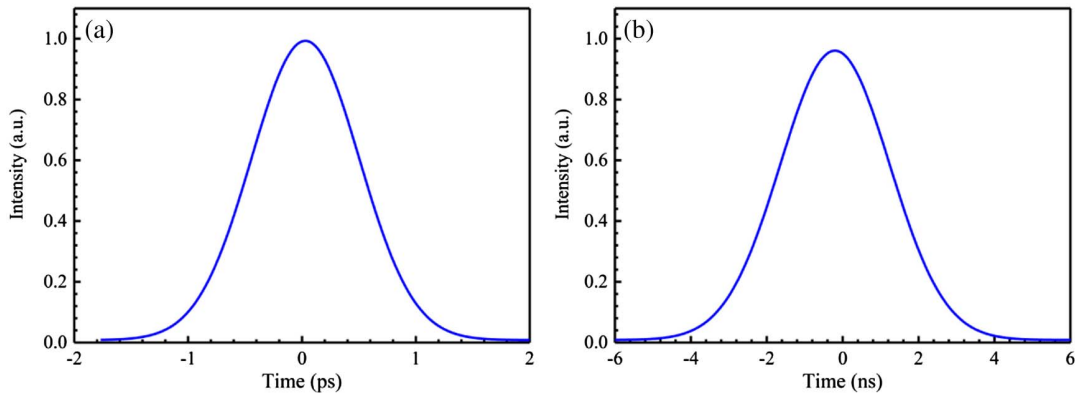

Fig. 5. (a) Output of a mode-locked pulse laser, measured by a second-order autocorrelator. (b) Output of a mode-locked pulse laser after the dispersive manipulation, recorded by the single-photon detection and a TDC.

coincidence counts. The HOM-dip can be observed in the HOM interference curve, i.e., coincidence counts versus the relative time delay between two arms of the HOM interferometer.

To demonstrate the ability of HOM interference in measuring the original width of laser pulses after dispersive manipulation, we insert a 50 km long fiber spool between the mode-locked laser and the VOA1 in Fig. 2 to introduce a remarkable dispersion before the laser pulses entering the HOM interferometer. The pulse width after such dispersive manipulation is directly measured through the single-photon detection and a TDC. The measured results are shown in Fig. 5(b). It shows that after propagating along a 50 km long fiber, the laser pulses have been broadened to 3.4 ± 0.3 ns, including a time jitter of the SNSPD and TDC.

Disclosures. The authors declare no conflicts of interest.

Data Availability. Data underlying the results presented in this paper are not publicly available at this time but may be obtained from the authors upon reasonable request.

REFERENCES

1. J. Bennett, R. B. Patel, C. A. Nicoll, D. A. Ritchie, and A. J. Shields, "Interference of dissimilar photon sources," Nat. Phys. **5**, 715–717 (2009).
2. J. Menssen, A. E. Jones, B. J. Metcalf, M. C. Tichy, S. Barz, W. S. Kolthammer, and I. A. Walmsley, "Distinguishability and many-particle interference," Phys. Rev. Lett. **118**, 153603 (2017).
3. J. S. Tang, Y. L. Li, X. Y. Xu, G. Y. Xiang, C. F. Li, and G. C. Guo, "Realization of quantum Wheeler's delayed-choice experiment," Nat. Photonics **6**, 600–604 (2012).
4. A. Peruzzo, P. Shadbolt, N. Brunner, S. Popescu, and J. L. O'Brien, "A quantum delayed-choice experiment," Science **338**, 634–637 (2012).
5. F. Kaiser, T. Coudreau, P. Milman, D. B. Ostrowsky, and S. Tanzilli, "Entanglement-enabled delayed-choice experiment," Science **338**, 637–640 (2012).
6. S. P. Walborn, A. N. de Oliveira, S. Padua, and C. H. Monken, "Multimode Hong-Ou-Mandel interference," Phys. Rev. Lett. **90**, 143601 (2003).
7. Z. Y. Ou, "Temporal distinguishability of an *N*-photon state and its characterization by quantum interference," Phys. Rev. A **74**, 063808 (2006).
8. E. Moschandreou, J. I. Garcia, B. J. Rollick, B. Qi, R. Pooser, and G. Siopsis, "Experimental study of Hong-Ou-Mandel interference using independent phase randomized weak coherent states," J. Lightwave Technol. **36**, 3752–3759 (2018).
9. R. B. Jin, T. Gerrits, M. Fujiwara, R. Wakabayashi, T. Yamashita, S. Miki, H. Terai, R. Shimizu, M. Takeoka, and M. Sasaki, "Spectrally

resolved Hong-Ou-Mandel interference between independent sources," Opt. Express **23**, 28836–28848 (2015).
10. T. Kobayashi, R. Ikuta, S. Yasui, S. Miki, T. Yamashita, H. Terai, T. Yamamoto, M. Koashi, and N. Imoto, "Frequency-domain Hong-Ou-Mandel interference," Nat. Photonics **10**, 441–444 (2016).
11. L. Y. Qu, J. Cotler, F. Ma, J. Y. Guan, M. Y. Zheng, X. P. Xie, Y. A. Chen, Q. Zhang, F. Wilczek, and J. W. Pan, "Color erasure detectors enable chromatic interferometry," Phys. Rev. Lett. **123**, 243601 (2019).
12. A. Lyons, T. Roger, N. Westerberg, S. Vezzoli, C. Maitland, J. Leach, M. J. Padgett, and D. Faccio, "How fast is a twisted photon?" Optica **5**, 682–686 (2018).
13. R. Valivarthi, M. G. Puigibert, Q. Zhou, G. H. Aguilar, V. B. Verma, F. Marsili, M. D. Shaw, S. W. Nam, D. Oblak, and W. Tittle, "Quantum teleportation across a metropolitan fibre network," Nat. Photonics **10**, 676–680 (2016).
14. Q. C. Sun, Y. L. Mao, S. J. Chen, W. Zhang, Y. F. Jiang, Y. B. Zhang, W. J. Zhang, S. Miki, T. Yamashita, H. Terai, X. Jiang, T.-Y. Chen, L.-X. You, X.-F. Chen, Z. Wang, J.-Y. Fan, Q. Zhang, and J.-W. Pan, "Quantum teleportation with independent sources and prior entanglement distribution over a network," Nat. Photonics **10**, 671–675 (2016).
15. H. L. Yin, T. Y. Chen, Z. W. Yu, H. Liu, L. X. You, Y. H. Zhou, S. J. Chen, Y. Q. Mao, M. Q. Huang, W. J. Zhang, H. Chen, M. J. Li, D. Nolan, F. Zhou, X. Jiang, Z. Wang, Q. Zhang, X.-B. Wang, and J.-W. Pan, "Measurement-device-independent quantum key distribution over a 404 km optical fiber," Phys. Rev. Lett. **117**, 190501 (2016).
16. A. Rubenok, J. A. Slater, P. Chan, I. Lucio-Martinez, and W. Tittel, "Real-world two-photon interference and proof-of-principle QKD immune to detector attacks," Phys. Rev. Lett. **111**, 130501 (2013).
17. Z. Y. Tang, Z. F. Liao, F. H. Xu, B. Qi, L. Qian, and H. K. Lo, "Experimental demonstration of polarization encoding measurement-device-independent quantum key distribution," Phys. Rev. Lett. **112**, 190503 (2014).
18. S. Y. Baek, O. Kwon, and Y. H. Kim, "Nonlocal dispersion control of a single-photon waveform," Phys. Rev. A **78**, 013816 (2008).
19. J. D. Franson, "Nonlocal cancellation of dispersion," Phys. Rev. A **45**, 3126–3132 (1992).
20. A. M. Steinberg, P. G. Kwiat, and R. Y. Chiao, "Dispersion cancellation and high-resolution time measurements in a fourth-order optical interferometer," Phys. Rev. A **45**, 6659–6665 (1992).
21. A. M. Steinberg, P. G. Kwiat, and R. Y. Chiao, "Dispersion cancellation in a measurement of the single-photon propagation velocity in glass," Phys. Rev. Lett. **68**, 2421–2424 (1992).
22. T. B. Pittman, D. V. Strekalov, A. Migdall, M. H. Rubin, A. V. Sergienko, and Y. H. Shih, "Can two-photon interference be considered the interference of two photons?" Phys. Rev. Lett. **77**, 1917–1920 (1996).
23. D. V. Strekalov, T. B. Pittman, and Y. H. Shih, "What we can learn about single photons in a two-photon interference experiment," Phys. Rev. A **57**, 567–570 (1998).
24. K. J. Blow, R. Loudon, and S. J. D. Phoenix, "Continuum fields in quantum optics," Phys. Rev. A **42**, 4102–4114 (1990).
25. K. Molmer, Y. Castin, and J. Dalibard, "Monte Carlo wave-function method in quantum optics," J. Opt. Soc. Am. B. **10**, 524–538 (1993).
26. W. J. Zhang, L. X. You, H. Li, J. Huang, C. L. Lv, L. Zhang, X. Y. Liu, J. J. Wu, Z. Wang, and X. M. Xie, "NbN superconducting nanowire single photon detector with efficiency over 90% at 1550 nm wavelength operational at compact cryocooler temperature," Sci. China Phys. Mech. Astron. **60**, 120314 (2017).
27. X. X. Ma, X. Y. Li, L. Cui, X. S. Guo, and L. Yang, "Effect of chromatic-dispersion-induced chirp on the temporal coherence properties of individual beams from spontaneous four-wave mixing," Phys. Rev. A **84**, 023829 (2011).
28. X. X. Ma, L. Cui, and X. Y. Li, "Hong-Ou-Mandel interference between independent sources of heralded ultrafast single photons: influence of chirp," J. Opt. Soc. Am. B **32**, 946–954 (2015).
29. J. G. Rarity, P. R. Tapster, and E. Jakeman, "Two-photon interference in a Mach-Zehnder interferometer," Phys. Rev. Lett. **65**, 1348–1351 (1990).
30. B. Liu and Z. Y. Ou, "Engineering multiphoton entangled states by quantum interference," Phys. Rev. A **74**, 035802 (2006).

31. I. Afek, O. Ambar, and Y. Silberberg, "High-NOON states by mixing quantum and classical light," Science **328**, 879–881 (2010).
32. L. A. Rozema, J. D. Bateman, D. H. Mahler, R. Okamoto, A. Feizpour, A. Hayat, and A. M. Steinberg, "Scalable spatial superresolution using entangled photons," Phys. Rev. Lett. **112**, 223602 (2014).
33. J. S. Sidhu and P. Kok, "Quantum metrology of spatial deformation using arrays of classical and quantum light emitters," Phys. Rev. A **95**, 063829 (2016).
34. Y. Miyamoto, T. Kuga, M. Baba, and M. Matsuoka, "Measurement of ultrafast optical pulses with two-photon interference," Opt. Lett. **18**, 900–902 (1993).
35. M. Maier, W. Kaiser, and J. A. Giordmaine, "Intense light bursts in the stimulated Raman effect," Phys. Rev. Lett. **17**, 1275–1277 (1966).
36. T. Legero, T. Wilk, A. Kuhn, and G. Rempe, "Time-resolved two-photon quantum interference," Appl. Phys. B **77**, 797–802 (2003).
37. T. Legero, T. Wilk, M. Hennrich, G. Rempe, and A. Kuhn, "Quantum beat of two single photons," Phys. Rev. Lett. **93**, 070503 (2004).
38. Y. S. Kim, O. Slattery, P. S. Kuo, and X. Tang, "Conditions for two-photon interference with coherent pulses," Phys. Rev. A **87**, 063843 (2013).
39. L. G. Cohen and C. Lin, "Pulse delay measurements in the zero material dispersion wavelength region for optical fibers," Appl. Opt. **16**, 3136–3139 (1977).
40. T. Ozeki and A. Watanabe, "Measurements of wavelength dependence of group delay in a multimode silica fiber," Appl. Phys. Lett. **28**, 382–383 (1976).
41. S. Diddams and J. C. Diels, "Dispersion measurements with white-light interferometry," J. Opt. Soc. Am. B **13**, 1120–1129 (1996).
42. L. G. Cohen, "Comparison of single-mode fiber dispersion measurement techniques," J. Lightwave Technol. **3**, 958–966 (1985).
43. Z. Y. Ou, E. C. Gage, B. E. Magill, and L. Mandel, "Fourth-order interference technique for determining the coherence time of a light beam," J. Opt. Soc. Am. B **6**, 100–103 (1989).
44. D. G. Im, Y. Kim, and Y. H. Kim, "Dispersion cancellation in a quantum interferometer with independent single photons," Opt. Express **29**, 2348–2363 (2021).